ACS APPLIED MATERIALS & INTERFACES

Research Article

www.acsami.org

Synthesis and Characterization of Sulfated TiO_2 Nanorods and ZrO_2/TiO_2 Nanocomposites for the Esterification of Biobased Organic Acid

Zhonglai Li, Renata Wnetrzak, Witold Kwapinski, and James J. Leahy*

Chemical and Environmental Science, University of Limerick, Ireland

ABSTRACT: TiO_2 nanorods and ZrO_2-modified TiO_2 nanocomposites have been prepared by hydrothermal synthesis and the deposition-precipitation method. Their sulfated products were tested as solid superacid catalysts for the esterification of levulinic acid which was used as a model bio-oil molecule. SEM and TEM characterization showed that TiO_2 nanorods with diameters ranging from 20 to 200 nm and with lengths of up to 5 μm were synthesized by a hydrothermal method at 180 °C. ZrO_2 nanoparticles with the diameters ranging from 10 to 20 nm were evenly deposited on TiO_2 nanorods. IR and XPS results suggested that sulfated ZrO_2/TiO_2 nanocomposite has higher content of sulfate groups on the surface with a S/(Zr+Ti) ratio of 13.6% than sulfated TiO_2 nanorods with a S/Ti ratio of 4.9%. The HPLC results showed that sulfated ZrO_2/TiO_2 nanocomposite have enhanced catalytic activity for esterification reaction between levulinic acid and ethanol compared to sulfated TiO_2 nanorods. The conversion of levulinic acid to ethyl levulinate can reach to 90.4% at the reaction temperature of 105 °C after 180 min.

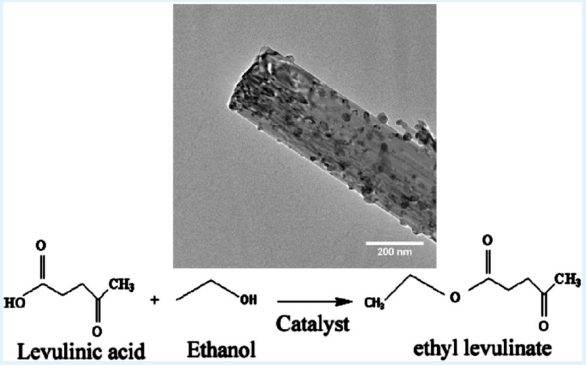

KEYWORDS: *ZrO_2, TiO_2, nanocomposite, sulfate, bio-oil, levulinic acid*

INTRODUCTION

There is currently significant interest in the preparation of nanostructure materials because of their unique optical, electronic and mechanical properties as well as their potential application as catalysts, sensors, or high efficiency solar cells.[1−3] Both TiO_2 and ZrO_2 as well as their nanostructured composites have been synthesized with a range of morphologies such as nanorods, nanotubes and nanoparticles and are used in dye-sensitized solar cells, gas sensors, energy storage devices and as catalysts for photocatalytic water splitting and the conversion of aldehydes to 1,1 diacetates.[4−8] The performance of these materials depends on specific morphological properties of the materials such as porosity and specific surface area as well as surface chemistry. Acid-modified zirconia and titania offer considerable potential as catalytic materials.[9−13] For example, Lin et al.[14] synthesized sulfated TiO_2 nanotubes and used them as catalysts for the esterification of acetic acid using cyclohexanol. These sulfated TiO_2 nanotubes demonstrated high activity for acetic acid conversion, whereas the anatase TiO_2 powder used for the preparation of nanotubes showed no catalytic activity. Sulfated ZrO_2 and other oxides such as Al_2O_3, SiO_2 and ZnO powders have also been used as the catalysts for the esterification of salicylic acid with phenol or the fatty acids in crude palm kernel oil and crude coconut oil.[15,16] Within these oxides, sulfated ZrO_2 catalyst showed higher catalytic activity for the conversion of organic acids than the other sulfated oxides acid catalysts.

Recently, bio-oil obtained by the pyrolysis of biomass has been suggested as an alternative source of gasoline and diesel.[17−20] However, these bio-oils consist of highly oxygenated organic species such as carboxylic acids, phenols and aldehydes. The reported oxygen contents for crude pyrolysis bio-oils are 20−40 wt %. resulting in a material that is water miscible with significantly lower heating value than mineral oil, low pH, and high viscosity, which makes storage and combustion problematic.[21−23] One promising route to improve some of these undesirable characteristics is through catalytic esterification of the organic acid with alcohol,[23−26] which requires catalytic materials with high activity that are easily recovered and regenerated.

To the best of our knowledge, there are no reports in the literature of the synthesis and sulfate groups modification of ZrO_2/TiO_2 nanocomposites with one-dimensional structure and their application as the catalysts for esterification of organic acids of levulinic acid, where most of reactions were carried out on powder catalysts such as silica-included Wells−Dawson heteropolyacid and dodecatungestophosphoric acid supported on acid-treated clay montmorillonite.[27,28]

Therefore, the objective of the work reported here is the synthesis and characterization of ZrO_2/TiO_2 nanocomposite and investigation of their catalytic activity for the esterification of levulinic acid. We report the synthesis of TiO_2 nanorods and ZrO_2−TiO_2 nanocomposites produced by hydrothermal and deposition−precipitation methods as well as their characterization and application as superacid catalysts for the esterification

Received: March 22, 2012
Accepted: August 14, 2012
Published: August 14, 2012

   dx.doi.org/10.1021/am300510u | *ACS Appl. Mater. Interfaces* 2012, 4, 4499−4505

of a model organic acid found in bio-oil. The model used was levulinic acid as it has been found in most of bio-oils generated by pyrolysis of biomass as well as being one of the primary products of the chemical hydrolysis of lignocellulosic biomass.[29,30]

EXPERIMENTAL SECTION

Preparation of Nanomaterials and Catalytic Esterification Reaction. TiO_2 nanorods were synthesized by a hydrothermal synthesis approach, which has been described in detail elsewhere.[31] Two grams of TiO_2 powder (Sigma-Aldrich) was mixed with 80.0 mL of 10.0 M NaOH solution, followed by hydrothermally treating the mixture at 180 °C for 48 h. Subsequently, the resulting powder was washed with 1.0 M HCl and water until it was pH neutral followed by calcination at 400 °C for 3 h.

ZrO_2/TiO_2 nanocomposites were prepared by a wet-chemical deposition precipitation (DP) method using the following procedure. 0.5230 g of zirconium(IV) oxychloride octahydrate ($ZrOCl_2 \cdot 8H_2O$, Sigma-Aldrich purity >99%) was dissolved in 50 mL of distilled water and mixed with TiO_2 nanorods, and sufficient NH_4OH was added to adjust the pH to about 11 to form a $Zr(OH)_4$ sol. This mixture was ultrasonicated to form a homogeneous slurry. The slurry was dried overnight at 105 °C before being calcined at 400 °C for 3 h to generate ZrO_2/TiO_2 nanocomposite. The nominal content of ZrO_2 was 20% by weight. The sulfated product was prepared by immersing the TiO_2 nanorods and ZrO_2/TiO_2 nanocomposite in 1.0 M H_2SO_4 solution for 3 h. The resulting products were calcined in a furnace at 500 °C for 5 h.

The esterification of levulinic acid was carried out in a 250 mL round-bottomed three-neck flask. 15.00 g of levulinic acid, 15.00 g of ethanol and 0.50 g of sulfated nanocomposite catalyst were added to the flask which was fitted with a reflux condenser with a temperature of −15 °C, and ethylene glycol was used as coolant for the condensor. After completion of the reaction, the catalyst was recovered by the filtration.

Characterization of Nanomaterials and Product Analysis. The amount of sulfate groups on the material was determined volumetrically by the adsorption of sodium hydroxide solution. About 0.05 g of the solid oxide and 3.0 g NaCl, which was used as an ion-exchange agent for sulfate groups, were shaken in 40 mL of H_2O for 10 h. The resulting suspension was then titrated by the dropwise addition of 0.0001 M NaOH (aq). The BET specific surface area (S_{BET}) of the material was carried out on a Micrometrics ASAP 2010 System. All the samples were degassed at 250 °C prior to nitrogen adsorption measurements. BET surface area was determined by a multipoint BET method using the adsorption data in the relative pressure (P/P_0) range of 0.05−0.3.

Powder X-ray diffraction (XRD) was obtained using Cu$K\alpha$ radiation in a Philip X'Pert diffactometer to identify the different phases and the crystal structure. The tube current was 40 mA and tube voltage was 40 kV. Scanning electron microscopy (SEM) was performed using a SU-70 SEM (Hitachi), operated at 3 kV. In order to avoid serious charging effects on the electron micrograph images, a layer of Au was deposited on the sample surface to improve conductivity. Transmission electron microscopy (TEM) was conducted at 200 kV using a JEOL-2010 equipped with energy-dispersive X-ray analysis (EDX). Samples for TEM analysis were prepared by drying sample materials-ethanol inks on amorphous carbon coated copper grids.

Raman spectra were recorded on a Dilor XY Labram spectrometer using a 514 nm green laser with 450 μm confocal hole and 150 μm confocal slit to minimize noise. A Bomen MB100 spectrometer was used to record the infrared spectra. X-ray Photoelectron Spectroscopy (XPS) analysis was conducted using an AXIS 165 X-ray photoelectron spectrometer and adventitious carbon was used as reference to correct the binding energy of the different samples. A Waters 510 HPLC with a UV−vis detector (430 nm) fitted with a Waters Novapak C_{18} column was employed to determine the concentration of levulinic acid. 5.0 mM aqueous H_2SO_4 was used as the mobile phase with a volumetric flow rate of 0.8 mL.min^{-1} and the operating temperature was 25 °C. The identification of the products following esterification was undertaken using a gas chromatography/mass spectrometer (GC/MS, Agilent 7890A/5975A).

RESULTS AND DISCUSSION

Structure Characterization of Material. XRD, SEM, and TEM were used to examine the phase structure and crystallite

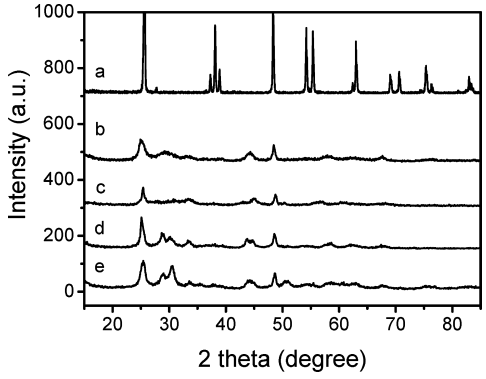

Figure 1. X-ray diffraction patterns of (a) TiO_2 powder, (b) TiO_2 nanorods, (c) sulfated TiO_2 nanorods, (d) 20 wt % ZrO_2/TiO_2 nanocomposite, and (e) sulfated 20 wt % ZrO_2/TiO_2 nanocomposite.

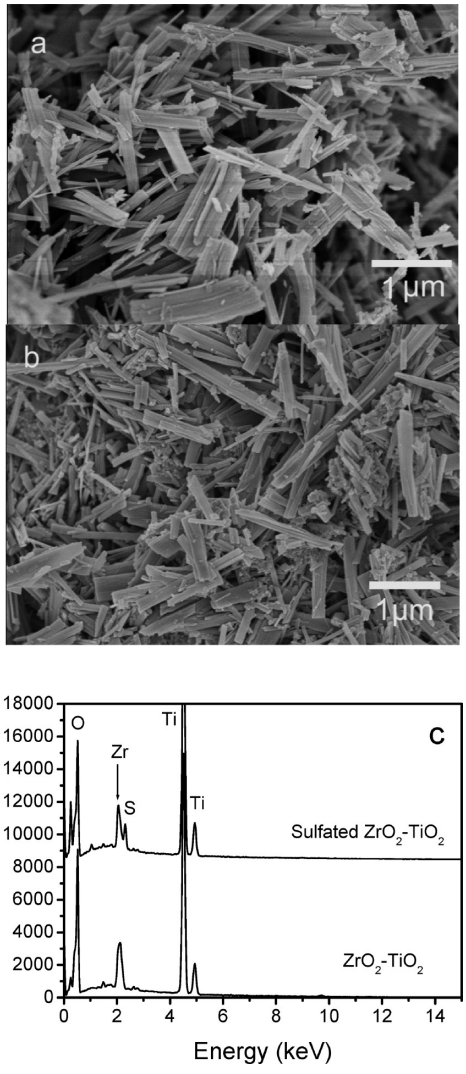

Figure 2. SEM images of (a) ZrO_2/TiO_2 nanocomposite, (b) sulfated ZrO_2/TiO_2 nanocomposite, and (c) EDX analysis of ZrO_2/TiO_2 nanocomposite with/without sulfate (SO_4^{2-}) functional groups.

dx.doi.org/10.1021/am300510u | ACS Appl. Mater. Interfaces 2012, 4, 4499−4505

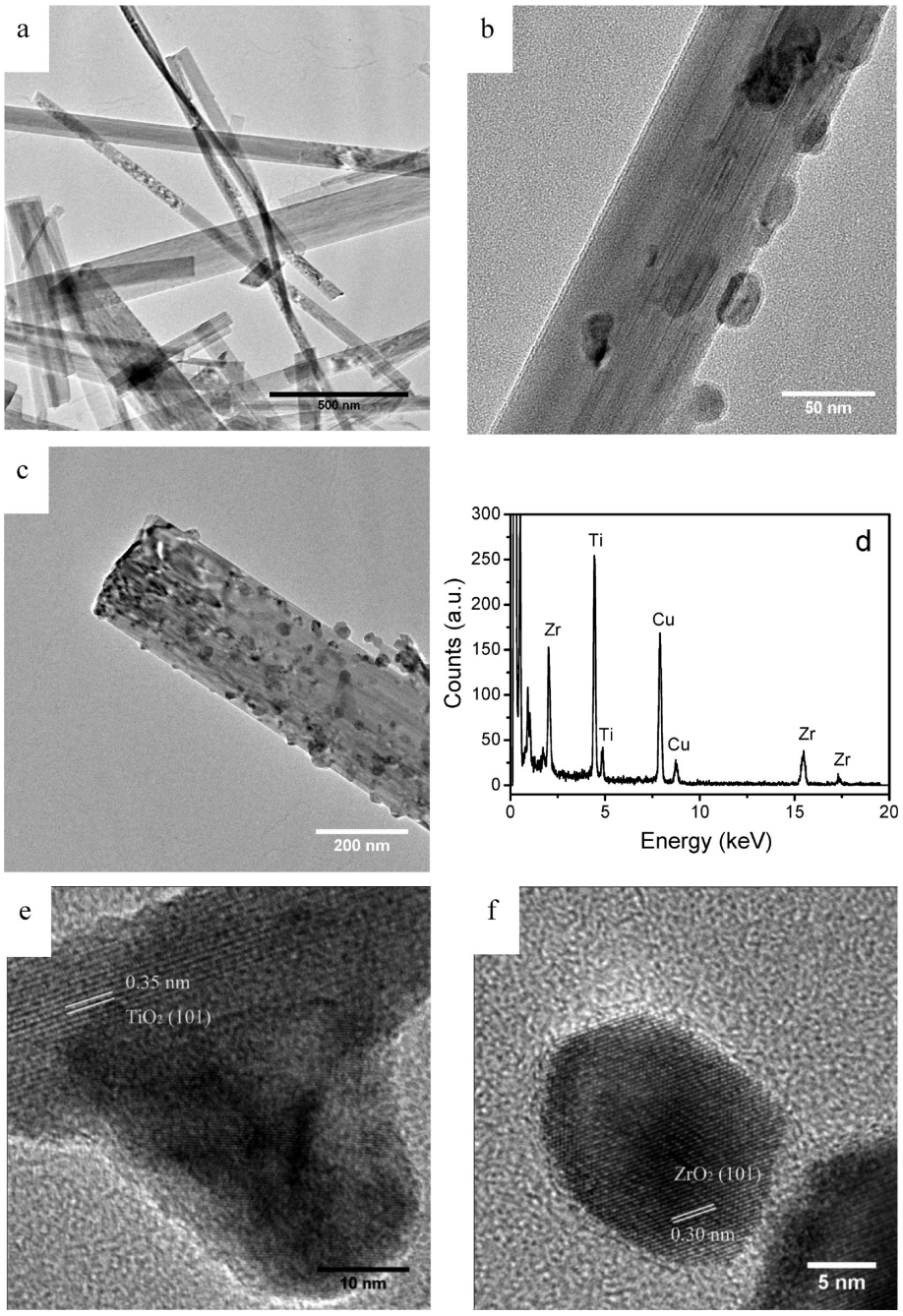

Figure 3. TEM images of (a) TiO_2 nanorods and (b, c) ZrO_2/TiO_2 nanocomposite with nominal loading amount of ZrO_2 of (b) 10 and (c) 20 wt %; (d) EDX spectrum of TiO_2/ZrO_2 composite; (e, f) high-resolution TEM images of (e) TiO_2 and (f) ZrO_2 nanoparticle.

size of synthesized materials. Figure 1 shows the XRD patterns of the TiO_2 powder used as a starting material, the TiO_2 nanorods, sulfated TiO_2 nanorods and sulfated ZrO_2/TiO_2 nanocomposite treated at 500 °C for 5 h. For the TiO_2 powder (Figure 1a), the peaks at 2θ = 25.4, 37.8, 48.5, 54.19, 55.37, and 62.99° are all attributable to the anatase phase of TiO_2, (JCPDS: 02−0406, 21−1272). The peaks at 2θ = 27.73° and 36.30° with lower intensity are due to the reflections of the rutile crystal structure.

The XRD of the sulfated TiO_2 nanorods presented in Figure 1c shows that the sulfated TiO_2 nanorods produced by washing the as-synthesized products with 1.0 M HCl to remove doped Na still retain the anatase crystal structure, suggesting dilute sulphuric acid did not alter the structure of TiO_2. However, the intensities of most of the peaks were reduced in intensity and the peaks corresponding to the rutile crystal structure disappeared, which may be due to rebuilding of the TiO_2 structure. This observation is similar to that of Kolen'Ko et al.,[32] who reported that following the hydrothermal synthesis of TiO_2 nanorods the structure of TiO_2 had been altered because of the formation of a Na-doped TiO_2 compound. Compared with the diffraction peaks of the TiO_2 powder and sulfated TiO_2 nanorods, the XRD pattern of the sulfated ZrO_2/TiO_2 nanocomposite shows two obvious ZrO_2 bands at 28.8° and 30.4°, which are assigned to the coexistence of monoclinic and tetragonal crystals of the ZrO_2 structure.[33]

SEM images of TiO_2 nanorods, ZrO_2/TiO_2 nanocomposite and the sulfated ZrO_2/TiO_2 nanocomposite are presented in Figure 2 and show nanorods distributed on the surface of

dx.doi.org/10.1021/am300510u | ACS Appl. Mater. Interfaces 2012, 4, 4499−4505

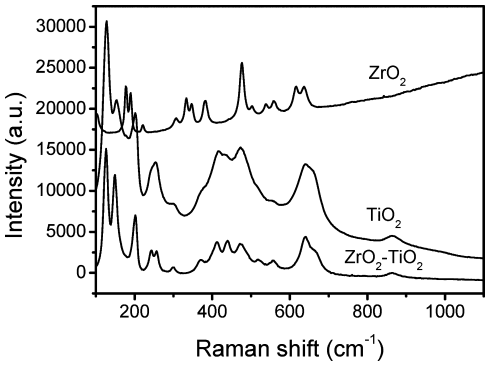

Figure 4. Raman spectra of (a) pure ZrO_2 powder, (b) sulfated TiO_2, and (c) sulfated ZrO_2/TiO_2 nanocomposite calcined at 500 °C for 5 h.

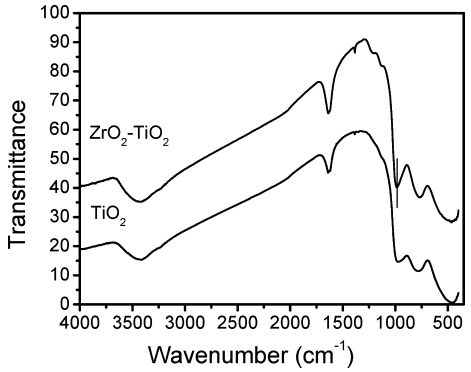

Figure 5. IR spectra of sulfated TiO_2 nanorods and sulafted ZrO_2/TiO_2 nanocomposite.

substrate with few particles. No obvious difference in the morphology of ZrO_2/TiO_2 nanocomposite and sulfated ZrO_2/TiO_2 nanocomposite was observed from the SEM images. The SEM images show that the majority of nanorods are between 1.0 and 5.0 μm in length and some nanorods are gathered into bundles. EDX analysis, presented in Figure 2c clearly shows that Ti, Zr and S are present on the nanocomposites depending on whether they are sulfated or not. In the EDX spectrum, the bands at 4.52 and 4.94 keV can be attributed to Ti Kα and Kβ, the band at 2.06 keV to Zr Lα1, and a weak band at 2.32 keV is attributed to S Kα.[34−36] These results are consistent with the formation of ZrO_2-decorated TiO_2 nanocomposite modified by surface sulfate groups.

Compared with SEM, TEM can provide higher resolution information regarding the surface morphologies and particle sizes of the nanocomposites. Typical morphology of the TiO_2 nanorods and the ZrO_2/TiO_2 nanocomposites are shown in Figure 3. The nanorods have lengths of up to 1.0 μm and the diameters of nanorods presented in Figure 3a range from 20 to 200 nm. The ZrO_2/TiO_2 nanocomposite with 20 wt % nominal loading of ZrO_2 in Figure 3c, show a significantly greater number of ZrO_2 nanoparticles with uniform diameters of 10−20 nm compared to the TiO_2 nanorods with 10 wt % ZrO_2 loading Figure 3b. An increase in ZrO_2 particle size was also observed with increased loading. The corresponding EDX analysis of TiO_2 supported ZrO_2 nanoparticles shown in Figure 3d also implies the presence of Ti and Zr elements. The crystalline nature of the ZrO_2/TiO_2 nanocomposites was also investigated by high resolution TEM (HRTEM). The HRTEM image presented in Figure 3e shows the surface of a nanorod with the lattice spacing of 0.35 nm being assigned to the (101) plane of the anatase phase. The HRTEM image in Figure 3f confirmed the formation of a ZrO_2 phase of about 20 nm in diameter and the observed lattice spacing of 0.30 nm on the nanoparticle matches well with the reported value of the (101) plane in the ZrO_2 tetragonal structure.[37]

Figure 4 shows the Raman spectra of the sulfated TiO_2 nanorods and the sulfated ZrO_2/TiO_2 nanocomposites calcined at 500 °C. The Raman bands at 127, 153, 201, 253, 414, 473, and 639 cm^{-1} are assigned to the anatase structure while the composite of ZrO_2 nanoparticles supported on TiO_2 nanorods show similar Raman bands at 126, 152, 201, 242, 256, 299, 370, 411, 439, 471, 519, 557, and 640 cm^{-1}. No obvious Raman bands for ZrO_2 were observed. However, the intensity ratio of the TiO_2 band at 127 cm^{-1} to that at 153 cm^{-1} in the composite is stronger than that of sulfated TiO_2 nanorods due to the fact that ZrO_2 inhibits changes in the phase structure of TiO_2 from anatase to rutile during calcination of the anatase phase at high temperatures.[38]

It is reported that the Raman bands of sulfate groups and Zr species are observed at 1030 cm^{-1} for SO_4^{2-} groups, at 180, 188, 221, 331, 380, 476, and 637 cm^{-1} for monoclinic phase and at 148, 290, 311, 454, and 647 cm^{-1} for tetragonal phase of ZrO_2, respectively.[39] However, we did not observe any peaks for ZrO_2 or the sulfate groups even though XRD, SEM and TEM show evidence of both species of ZrO_2 and sulfate groups, which suggests that the ZrO_2 particles are highly dispersed on the surface of the TiO_2 nanorods and the signals for ZrO_2 may be masked by those of TiO_2.

IR and XPS of the synthesized materials were also carried out as the Raman results did not provide any Zr and sulfur information. The infrared spectra of sulfated TiO_2 nanorods and sulfated ZrO_2/TiO_2 nanocomposites calcined at 500 °C are shown in Figure 5. A band at 980 cm^{-1} can be assigned to the symmetric stretching vibration of the S−O bond on sulfated TiO_2 nanorods and ZrO_2/TiO_2 nanocomposite.[40,41] However, two extra bands at 1135 and 1220 cm^{-1} are observed for ZrO_2/TiO_2 nanocomposites. The band around 1135 cm^{-1} is due to the symmetric stretching of the S═O bond and the band around 1220 cm^{-1} is attributed to asymmetric stretching of the S═O bond. These are the characteristic frequencies of a bridged bidentate SO_4^{2-} coordinated to Zr^{4+} and/or Ti^{4+}.[42] The IR results clearly indicate that TiO_2 nanorods and ZrO_2/TiO_2 nanocomposite have been successful modified by sulfate functional groups, and two potential catalytically active sites are present on ZrO_2/TiO_2 nanocomposite.

The intensity of both the 1135 and 1220 cm^{-1} bands of the sulfated ZrO_2/TiO_2 nanocomposite were stronger than those of sulfated TiO_2, indicating that the introduction of ZrO_2 increases the concentration of surface-adsorbed sulfate groups. Surface sulfate groups play an important role in heterogeneous catalysis by offering active acid sites. In addition, a weak IR band appeared at the higher S−O stretching frequency of 1380 cm^{-1}, which indicates that disulfate species are formed on ZrO_2/TiO_2 nanocomposite. It is worth to note that the amount of sulfate groups on newly prepared sulfated ZrO_2/TiO_2 nanocomposite is about 257.6 μmol/g, which corresponds to 1.71 SO_4 groups per nm^2 on the surface of nanocomposite. However, the amount of sulfate groups on sulfated TiO_2 nanorods is only 160.2 μmol/g, about 0.35 SO_4 groups per nm^2 on the surface of TiO_2. The calculation of surface coverage of SO_4 is obtained according to BET surface area of sulfated ZrO_2/TiO_2 nanocomposite of 15.0 m^2/g and sulfated TiO_2 nanorods of 45.4 m^2/g. A wide and weak band observed at 3420 cm^{-1} is attributed to the hydroxyl group

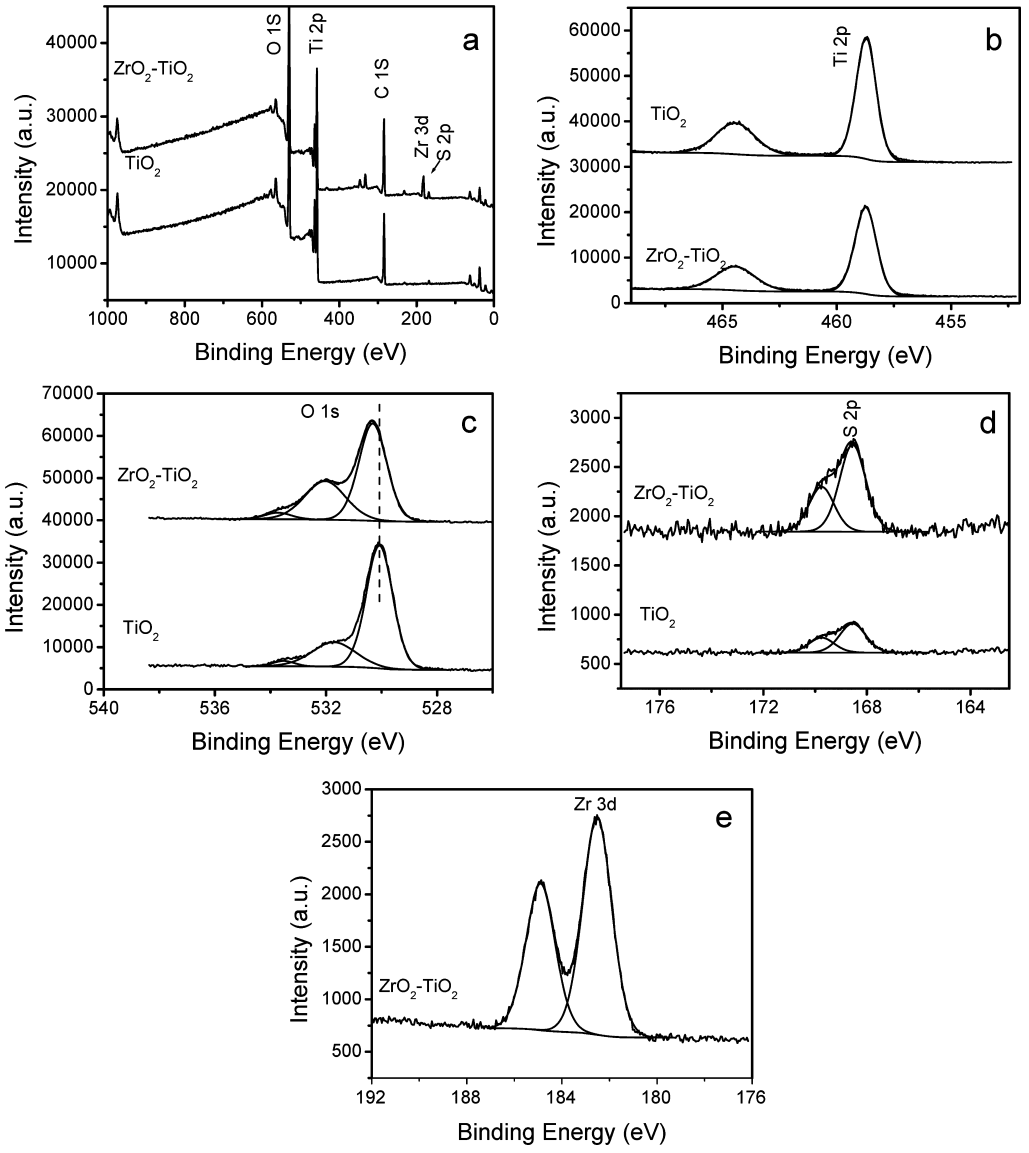

Figure 6. (a) Survey scan XPS spectra in the binding energy range 0−1000 eV and high-resolution spectra, (b) Ti 2p, (c) O 1s, (d) S 2p of sulfated TiO_2 nanorods and sulfated ZrO_2/TiO_2 nanocomposite, and (e) Zr 3d of sulfated ZrO_2/TiO_2 nanocomposite.

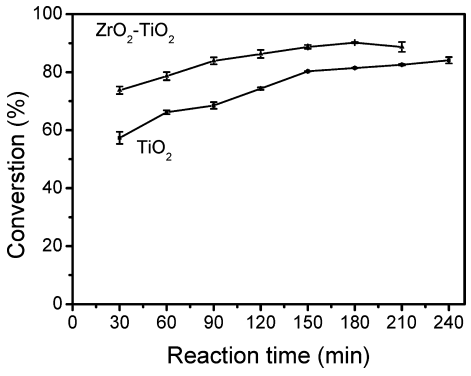

Figure 7. Effect of reaction time on levulinic acid conversion on (a) sulfated TiO_2 nanorods and (b) sulfated ZrO_2/TiO_2 nanocomposite at 105 °C. The ratio of LA to Ethanol is 1 by weight.

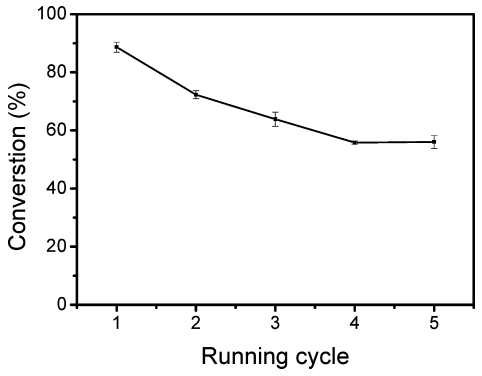

Figure 8. Reusability of sulfated ZrO_2−TiO_2 nanocomposite for multiple cycles.

stretching mode of water associated with zirconia/titania, while an intense band observed at 1635 cm^{-1} is assigned to the OH bending mode of water associated with the sulfate group.

Figure 6 shows the XPS spectra of the typical elements on sulfated TiO_2 nanorods and sulfated TiO_2−ZrO_2 nanorods calcined at 500 °C. The binding energies recorded for Ti 2p, O 1s, S 2p of sulfated TiO_2 nanorods are 458.7, 530.1, and 168.5 eV,

dx.doi.org/10.1021/am300510u | ACS Appl. Mater. Interfaces 2012, 4, 4499−4505

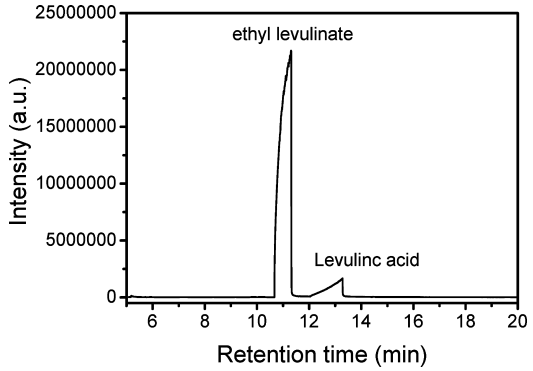

Figure 9. GC−MS spectroscopy of product and reactant after esterification reaction at 105 °C for 180 min.

respectively, whereas the binding energies of Ti 2p, O 1s, and S 2p of the sulfated ZrO_2/TiO_2 nanocomposite are at 458.8 eV, 530.3 and 168.7 eV, respectively. In contrast, Ti 2p, O 1s, Zr 3d of ZrO_2/TiO_2 nanocomposite without sulfur groups are at 457.9, 529.5, and 181.7 eV, respectively. The XPS spectra clearly indicate the presence of sulfur and S effect on the binding energies of O, Ti and Zr. However, it is believed that only one sulfur species of SO_4^{2-} on the materials. The increase in the binding energies of Ti, O and S are due to the stronger electron withdrawing ability of Ti, O and S in ZrO_2/TiO_2 nanocomposites. The measured binding energy of Zr $3d_{5/2}$ was 182.5 eV for the ZrO_2/TiO_2 nanocomposite and the binding energies of Zr and Ti corresponded to the tetragonal ZrO_2 and anatase TiO_2 phases, respectively.[43] In addition, XPS was used to investigate the atomic concentration ratios of sulfate groups present on the surfaces of TiO_2 nanorods and ZrO_2/TiO_2 nanocomposite. It was found that the S/(Zr+Ti) atomic ratio of 13.6% on sulfated ZrO_2/TiO_2 nanocomposite is much higher than that of sulfated TiO_2 nanorods with an atomic ratio of 4.9% corroborating the IR experimental results. The increase in the atomic surface concentration ratios of S/(Ti+Zr) can be explained by the appearance of ZrO_2 particles on the TiO_2 nanorods as ZrO_2 can stabilize more SO_4^{2-} functional groups than TiO_2.

Upgrading of Bio-oil Model Acid. The catalytic activity of the sulfated TiO_2 nanorods and ZrO_2/TiO_2 nanocomposite was investigated using esterification as a model reaction. Levulinic acid was used as a model compound as it is widely found in bio-oils produced from pyrolysis and is a primary output from chemical hydrolysis of lignocellulosic biomass. Figure 7 shows the catalytic conversion of levulinic acid on sulfated TiO_2 nanorods and ZrO_2/TiO_2 nanocomposite materials as a function of the reaction time. It can be seen that both sulfated TiO_2 nanorods and ZrO_2/TiO_2 nanocomposite show high catalytic activity for levulinic acid conversion at 105 °C, while blank experiments showed that the conversion of levulinic acid of lower than 2% was observed according to HPLC results. After 30 min reaction, almost 75% levulinic acid conversion on sulfated ZrO_2/TiO_2 nanocomposite is achieved, whereas about 60% levulinic acid conversion is observed for sulfated TiO_2. With an increase in reaction time from 30 to 210 min, both catalysts show an increased conversion of the levulinic acid. The reaction reached equilibrium for the sulfated ZrO_2/TiO_2 nanocomposite with a levulinic acid conversion of 90.4%, while in the case of the reaction catalyzed by sulfated TiO_2 nanorods equilibrium was not reached after 4 h but conversion was 83.2%. The results clearly show that the sulfated ZrO_2/TiO_2 nanocomposite materials exhibit increased catalytic activity for levulinic acid esterification compared to the sulfated TiO_2 nanomaterials.

The stability and recyclability of sulfated ZrO_2/TiO_2 nanocomposite was also investigated. The catalyst was recovered after each batch esterification reaction cycle by filtering, washing using ethanol, drying, and using the catalyst in the following reaction cycle. The results of esterification carried out using the catalyst for five consecutive reaction cycles under identical reaction conditions are shown in Figure 8. The sulfated ZrO_2/TiO_2 nanocomposite shows the highest conversion in the first reaction run but the conversion of levulinic acid to ester decrease with subsequent reaction cycles. After the five cycles, the conversion of levulinic acid has fallen from 90% to around 60%, suggesting that a significant amount of sulfate groups persisted on the surfaces of TiO_2 and ZrO_2 and served as the catalytically catalyst sites for esterification.

To investigate the nature of catalyst deactivation, we analyzed used sulfated ZrO_2/TiO_2 nanocomposite by XPS. The binding energies of Ti 2p, Zr 3d, and S 2p of sulfated ZrO_2/TiO_2 nanocomposite are at 458.7, 182.5, and 168.8 eV. There is a slightly peak shift for Ti and S when compared to newly prepared nanocomposite. Additionally, the amount change in surface sulfate groups between sulfated ZrO_2/TiO_2 nanocomposite and sulfated TiO_2 nanorods is compared before and after the reaction. The amount of sulfate groups on sulfated ZrO_2/TiO_2 nanocomposite decreases from 257.6 to 99.8 μmol/g, and the amount of sulfate group on sulfated TiO_2 nanorods decreases from 160.2 to 82.6 μmol/g. Therefore, the deactivation of the catalyst is mainly attributed to the loss of surface functional groups on the catalysts. According to XRD, IR, and TEM results, sulfate groups are found to be adsorbed on ZrO_2 with tetragonal and monoclinic structure. However, it is reported that sulfate groups on monoclinic structures are unstable and may be lost during the reaction and washing process.[44] GC-MS of the reaction products showed that only ethyl levulinate is obtained after the esterification at 105 °C for 180 min, as shown in Figure 9.

CONCLUSIONS

In summary, sulfated TiO_2 nanorods and ZrO_2-modified TiO_2 nanocomposites were prepared by hydrothermal and deposition-precipitation methods. The TiO_2 nanorods were found to have diameters ranging from 20 to 200 nm and lengths of up to 5 μm. ZrO_2 nanoparticles deposited on TiO_2 nanorods have diameters around 20 nm. Sulfate functional groups were adsorbed onto Ti and Zr sites on TiO_2 and ZrO_2/TiO_2 nanocomposites. Compared to sulfated TiO_2 nanorods with a S/Ti ratio of 4.9%, sulfated ZrO_2-modified TiO_2 nanocomposites delivered higher concentration of sulfate groups with a S/(Zr+Ti) ratio of 13.6%. ZrO_2-modified TiO_2 nanocomposites exhibited high catalytic activity for levulinic acid esterification and the conversion of levulinic acid can reach around 90% at 105 °C. Moreover, sulfated ZrO_2-modified TiO_2 nanocomposites demonstrated stability after several running cycles.

AUTHOR INFORMATION

Corresponding Author

*Tel.: +353 61 20 2649. Fax: +353 61 20 2568. E-mail: j.j.leahy@ul.ie.

Notes

The authors declare no competing financial interest.

■ ACKNOWLEDGMENTS

Z.L. thanks Dr. Calum for SEM and TEM analysis and Dr. Fathima for Raman measurements. This work was financially supported by the Enterprise Ireland (EI CC/2009/1305A).

■ REFERENCES

(1) Dongre, J. K.; Ramrakhiani, M. *J. Alloys Compd.* **2009**, *487*, 653−658.
(2) Kim, K. D.; Tai, W. S.; Kim, Y. D. *J. Nanosci. Nanotechnol.* **2010**, *10*, 375−379.
(3) Qureshi, A.; Kang, W. P.; Davidson, J. L.; Gurbuz, Y. *Diamond Relat. Mater.* **2009**, *18*, 1401−1420.
(4) Lan, Z.; Wu, J. H. *Prog. Chem.* **2010**, *22*, 2248−2253.
(5) He, X. S.; Hu, C. G.; Feng, B.; Wan, B. Y.; Tian, Y. S. *J. Electrochem. Soc.* **2010**, *157*, J381−J385.
(6) Zhou, H. S.; Li, D. L.; Hibino, M.; Honma, I. *Angew Chem., Int. Ed.* **2005**, *44*, 797−802.
(7) Allen, M. R.; Thibert, A.; Sabio, E. M.; Browning, N. D.; Larsen, D. S.; Osterloh, F. E. *Chem. Mater.* **2010**, *22*, 1220−1228.
(8) Reddy, B. M.; Sreekanth, P. M.; Khan, A. *Synth. Commun.* **2004**, *34*, 1839−1845.
(9) Lu, Q.; Xiong, W. M.; Li, W. Z.; Guo, Q. X.; Zhu, X. F. *Bioresour. Technol.* **2009**, *100*, 4871−4876.
(10) Krishnakumar, B.; Swaminathan, M. *J. Organomet. Chem.* **2010**, *695*, 2572−2577.
(11) Ropero-Vega, J. L.; Aldana-Perez, A.; Gomez, R.; Nino-Gomez, M. E. *Appl. Catal., A* **2010**, *379*, 24−29.
(12) Yang, D.; Li, J. H.; Wen, M. F.; Song, C. L. *Catal. Lett.* **2008**, *122*, 138−143.
(13) Wang, B.; Cui, X.; Ma, H. Z.; Li, J. *Energy Fuels* **2007**, *21*, 3748−3750.
(14) Lin, C. H.; Chien, S. H.; Chao, J. H.; Sheu, C. Y.; Cheng, Y. C.; Huang, Y. J.; Tsai, C. H. *Catal. Lett.* **2002**, *80*, 153−159.
(15) Kuriakose, G.; Nagaraju, N. *J. Mol. Catal. A: Chem.* **2004**, *223*, 155−159.
(16) Jitputti, J.; Kitiyanan, B.; Rangsunvigit, P.; Bunyakiat, K.; Attanatho, L.; Jenvanitpanjakul, P. *Chem. Eng. J.* **2006**, *116*, 61−66.
(17) Park, H. J.; Jeon, J. K.; Kim, J. M.; Lee, H. I.; Yim, J. H.; Park, J.; Park, Y. K. *J. Nanosci. Nanotechnol.* **2008**, *8*, 5439−5444.
(18) Briens, C.; Piskorz, J.; Berruti, F. *Int. J. Chem. React. Eng.* **2008**, *6*, R2.
(19) Laird, D. A.; Brown, R. C.; Amonette, J. E.; Lehmann, J. *Biofuels, Bioprod. Biorefin.* **2009**, *3*, 547−562.
(20) Lu, Q.; Li, W. Z.; Zhu, X. F. *Energ. Convers. Manage.* **2009**, *50*, 1376−1383.
(21) Garcia-Perez, M.; Chaala, A.; Roy, C. *J. Anal. Appl. Pyrolysis.* **2002**, *65*, 111−136.
(22) Xu, Y.; Wang, T. J.; Ma, L. L.; Zhang, Q.; Wang, L. *Biomass Bioenergy* **2009**, *33*, 1030−1036.
(23) Jiang, X. X.; Ellis, N. *Energy Fuels* **2010**, *24*, 1358−1364.
(24) Hilten, R. N.; Bibens, B. P.; Kastner, J. R.; Das, K. C. *Energy Fuels* **2010**, *24*, 673−682.
(25) Zhou, L.; Zong, Z. M.; Tang, S. R.; Zong, Y.; Xie, R. L.; Ding, M. J.; Zhao, W.; Zhu, X. F.; Xia, Z. L.; Wu, L.; Wei, X. Y. *Energy Sources A* **2010**, *32*, 370−375.
(26) Venderbosch, R. H.; Prins, W. *Biofuels, Bioprod. Biorefin.* **2010**, *4*, 178−208.
(27) Pasquale, G.; Vazquez, P.; Romanelli, G.; Baronetti, G. *Catal. Commun.* **2012**, *18*, 115−120.
(28) Dharne, S.; Bokade, V. V. *J. Nat. Gas Chem.* **2011**, *20*, 18−24.
(29) Alonso, D. M.; Bond, J. Q.; Dumesic, J. A. *Green Chem.* **2010**, *12*, 1493−1513.
(30) Lin, L.; He, B. H.; Sun, R. C.; Hu, R. F. *Prog. Chem.* **2007**, *19*, 1206−1216.
(31) Nian, J. N.; Teng, H. S. *J. Phys. Chem. B* **2006**, *110*, 4193−4198.
(32) Kolen'ko, Y. V.; Kovnir, K. A.; Gavrilov, A. I.; Garshev, A. V.; Frantti, J.; Lebedev, O. I.; Churagulov, B. R.; Van Tendeloo, G.; Yoshimura, M. *J. Phys. Chem. B* **2006**, *110*, 4030−4038.
(33) Zhang, X.; Wang, H.; Xu, B. Q. *J. Phys. Chem. B* **2005**, *109*, 9678−9683.
(34) Tsurui, T.; Wataru, M.; Watanabe, M.; Katsumata, T.; Inaguma, Y. *J. Electron Microsc. Relat. Phenom.* **2009**, *58*, 349−355.
(35) Rodrigo, K.; Knudsen, J.; Pryds, N.; Schou, J.; Linderoth, S. *Appl. Surf. Sci.* **2007**, *254*, 1338−1342.
(36) Li, L.; Lin, C. T. *Ind. Eng. Chem. Res.* **1994**, *33*, 3241−3246.
(37) Srinivasan, R.; Watkins, T. R.; Hubbard, C. R.; Davis, B. H. *Chem. Mater.* **1995**, *7*, 725−730.
(38) Zhang, J.; Li, M. J.; Feng, Z. C.; Chen, J.; Li, C. *J. Phys. Chem. B* **2006**, *110*, 927−935.
(39) Reddy, B. M.; Sreekanth, P. M.; Lakshmanan, P. *J. Mol. Catal. A: Chem.* **2005**, *237*, 93−100.
(40) Jariwala, M.; Crawford, J.; LeCaptain, D. J. *Ind. Eng. Chem. Res.* **2007**, *46*, 4900−4905.
(41) Morterra, C.; Cerrato, G.; Emanuel, C.; Bolis, V. *J. Catal.* **1993**, *142*, 349−367.
(42) Babou, F.; Coudurier, G.; Vedrine, J. C. *J. Catal.* **1995**, *152*, 341−349.
(43) Chang, S. M.; Doong, R. A. *J. Phys. Chem. B* **2006**, *110*, 20808−20814.
(44) Fan, G. D.; Shen, M.; Zhang, Z.; Jia, F. R. *J. Rare Earths* **2009**, *27*, 437−442.